ACS APPLIED MATERIALS & INTERFACES

www.acsami.org

Research Article

Identifying Physical and Chemical Contributions to Friction: A Comparative Study of Chemically Inert and Active Graphene Step Edges

Zhe Chen,[§] Arash Khajeh,[§] Ashlie Martini,* and Seong H. Kim*

Cite This: *ACS Appl. Mater. Interfaces* 2020, 12, 30007−30015

Read Online

ACCESS | Metrics & More | Article Recommendations | Supporting Information

ABSTRACT: Friction has both physical and chemical origins. To differentiate these origins and understand their combined effects, we study friction at graphene step edges with the same height and different terminating chemical moieties using atomic force microscopy (AFM) and reactive molecular dynamics (MD) simulations. A step edge produced by physical exfoliation of graphite layers in ambient air is terminated with hydroxyl (OH) groups. Measurements with a silica countersurface at this exposed step edge in dry nitrogen provide a reference where both physical topography effects and chemical hydrogen-bonding (H-bonding) interactions are significant. H-bonding is then suppressed in AFM experiments performed in alcohol vapor environments, where the OH groups at the step edge are covered with physisorbed alcohol molecules. Finally, a step edge buried under another graphene layer provides a chemically inert topographic feature with the same height. These systems are modeled by reactive MD simulations of sliding on an OH-terminated step edge, a step edge with alkoxide group termination, or a buried step edge. Results from AFM experiments and MD simulations demonstrate hysteresis in friction measured during the step-up versus step-down processes in all cases except the buried step edge. The origin of this hysteresis is shown to be the anisotropic deflection of terminal groups at the exposed step edge, which varies depending on their chemical functionality. The findings explain why friction is high on atomically corrugated and chemically active surfaces, which provides the insight needed to achieve superlubricity more broadly.

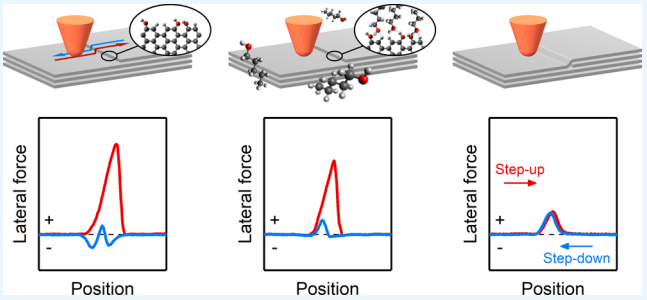

KEYWORDS: *friction, graphite, topographic corrugation, atomic force microscopy, reactive molecular dynamics*

INTRODUCTION

Friction, the resistance to the relative movement of two contiguous bodies, is a ubiquitous phenomenon occurring in both natural and engineering systems across length scales.[1−4] At the macroscale, Amontons' law predicts that friction between two solids is proportional to the applied normal force but independent of the contact area.[5,6] This observation is attributed to the fact that macroscopic objects are topographically corrugated such that only a few asperities are in contact and undergo physical deformation during contact and sliding.[7,8] At the nanoscale, atomic interactions at sliding interfaces dominate frictional phenomena, and the contact area becomes a significant factor.[9] Therefore, nanoscale friction behavior is no longer described by Amontons' law. For single-asperity contacts, if the surfaces are atomically smooth and chemically inert, continuum mechanics theories that incorporate adhesion can be used to model friction.[8,9] However, if the surfaces are atomically corrugated or there are chemical interactions between the contacting surfaces, continuum mechanics theories may no longer apply.[10−13] In such cases, a better understanding of the physical and chemical factors that affect friction is needed to efficiently control or mitigate friction-related interfacial processes. However, the fundamental mechanisms governing the magnitude of friction have remained elusive due to an incomplete understanding of the interplay between atomic-scale corrugation and chemical interactions within a contact region and difficulties associated with independently controlling or distinguishing such parameters in experiments.

These limitations can be circumvented by studying friction at well-defined atomic step edges on a single-crystalline graphite basal plane. These step edges occur at the border between the upper and lower basal planes of graphite. The basal plane of graphite is atomically flat, and the sp^2-hybridized carbon atoms arranged in the hexagonal array are chemically inert. Unless the countersurface is a crystallographically aligned

Received: May 3, 2020
Accepted: June 4, 2020
Published: June 4, 2020

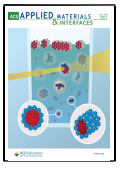

https://dx.doi.org/10.1021/acsami.0c08121
ACS Appl. Mater. Interfaces 2020, 12, 30007−30015

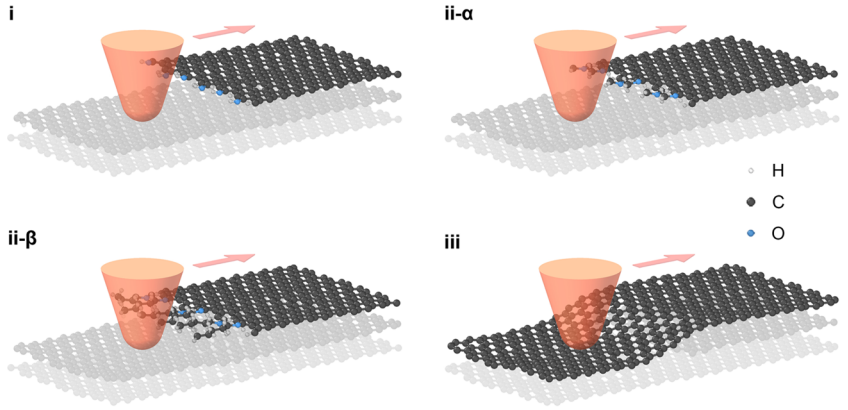

Figure 1. Illustrations of the systems studied. Each system comprises an AFM tip (countersurface) and a graphite surface with an atomic step edge whose height is 0.34 nm, corresponding to the thickness of a single graphene layer. (i) The graphene step edge is exposed and terminated with chemically active OH groups. (ii) The step edge is exposed and terminated with physisorbed alcohol molecules or chemisorbed alkoxide groups: short (ii-α) and long (ii-β) alkyl groups are considered. (iii) The step edge is buried under another graphene layer.

graphite plane, the atomic order of its surface will be incommensurate to the hexagonal lattice of the graphite.[14−16] Thus, friction on the graphite basal plane is ultralow,[17−19] making it easy to detect any minute increase in friction due to chemical or physical interactions at the termination of the basal plane. When the step edge is produced by mechanical exfoliation of a graphite basal plane in ambient air, reactions of the dangling bonds at the newly formed edge with water molecules impinging from the gas phase will produce hydroxyl (OH) groups chemically anchored to the step edge.[20,21] These OH groups can form transient hydrogen bonds (H-bonds) with the oxygen atoms or OH groups of the countersurface within the sliding contact region. Further, friction can be measured without any chemical interactions if the step edge is buried, i.e., covered with single-layer graphene.

These features make step edges at the graphite basal plane ideal for fundamental studies of friction.[22−25] Studies with a single-asperity countersurface of amorphous silica sliding on a buried step edge have shown that the resistive force due to the topographic height change during sliding from the lower terrace to the upper terrace (hereafter called "step-up") has the same magnitude as the assistive force in the opposite "step-down" scan direction.[26−29] In contrast, at exposed step edges terminated with OH functional groups, H-bonding interactions with the OH groups at the silica surface exert a resistive force during both step-up and step-down processes.[29,30] During the step-up process, both topographic (physical) and H-bonding (chemical) effects contribute to increasing friction. In contrast, during the step-down process, the two contributions have opposite effects and whether the overall force is resistive or assistive depends on which effect, the physical or the chemical, is larger.[29,30] In the previous studies, it was found that friction during step-up on an exposed step edge is much larger than the sum of the magnitudes of the chemical (resistive) and physical (assistive) forces during step-down. In other words, friction is not fully reversible during the step-up and step-down processes for the chemically active step edge, while it is fully reversible at the chemically inert buried step edge. Based on these comparisons, it was hypothesized that chemical interactions at the atomically corrugated topographic feature increase the step-up resistance much more than they increase the step-down assistance.[30] However, the mechanisms underlying the proposed friction amplification and hysteresis were not fully elucidated.

Here, we investigated the atomistic mechanisms governing the magnitude of friction during the step-up and step-down processes on a topographic step of a single-layer graphene edge (0.34 nm high) on a graphite basal plane. This system was studied experimentally using atomic force microscopy (AFM) with a sharp silicon tip covered with an amorphous native oxide layer and computationally using reactive molecular dynamics (MD) simulations. As shown in Figure 1, three different cases were studied: (i) graphene step edges with OH groups capable of H-bonding interactions, (ii) graphene step edges with hydrophobic species, and (iii) buried graphene step edges covered with another graphene layer. The second case was implemented by the physisorption of alcohol at the OH sites in experiments or chemisorption of alcohol via dehydration reaction with the OH group forming alkoxide groups in simulations. Depending on the size of the alkyl moiety of the alcohol molecule or the alkoxide group, the deformability of molecular species at the topographic step can vary. In our study, methanol (ii-α) and *n*-pentanol (ii-β) were used to model short and long alkyl chains at the step edge. Results revealed that, unless the topographic step is completely chemically inert, the resistive force during the step-up process is always larger than the assistive force during the step-down process. The magnitude of this hysteresis depends on the degree of the sliding direction-dependent physical deformation of molecular moieties at the topographic step, which in turn depends on their chemical interactions with the countersurface.

MATERIALS AND METHODS

Nanoscale Friction Measurement. A fresh graphite surface was prepared through tape exfoliation on a highly oriented pyrolytic graphite (HOPG) crystal in ambient air. Nanoscale friction tests were performed with AFM (Multimode, Bruker) using Si tips (ESP-V2, Bruker; nominal spring constant, 0.2 N/m; nominal tip radius, 8 nm) to rub against the fresh graphite surface in contact mode. The sliding direction of the AFM tip was kept nearly perpendicular to the graphene step edges. Before the friction test, the AFM tip was treated with UV/ozone for 15 min to remove possible organic contaminants. During the test, the reciprocating frequency of the tip was 2 Hz and the scan size was 80 nm, so the tip sliding speed was 0.32 μm/s. The applied normal force on the AFM tip was in the range of 7.8−23.5 nN. According to the Derjaguin−Muller−Toporov (DMT) contact model,[31] based on the nominal tip radius, the contact pressure varied between 2.2 and 2.7 GPa. The normal spring constant of the AFM

https://dx.doi.org/10.1021/acsami.0c08121
ACS Appl. Mater. Interfaces 2020, 12, 30007−30015

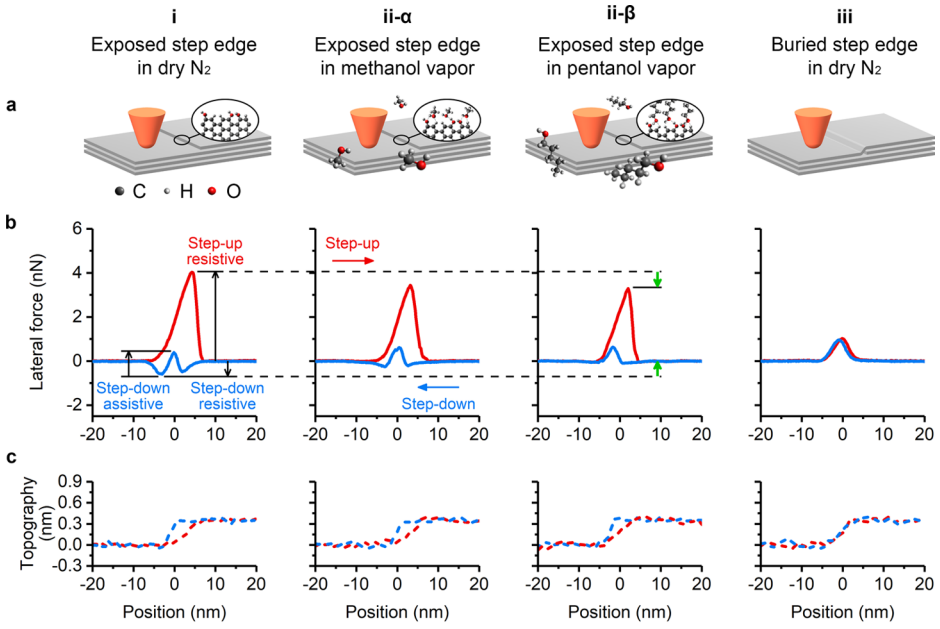

Figure 2. Experimental setup and results of the AFM-based nanoscale friction tests. (a) Illustration of four sets of friction tests in which a Si AFM tip slides over an exposed single-layer graphene step edge in (i) dry nitrogen, (ii-α) methanol vapor, and (ii-β) *n*-pentanol vapor, and (iii) the same Si tip sliding over a buried single-layer graphene step edge in dry nitrogen. (b) Lateral force for the tip sliding in the step-up (red) and step-down (blue) directions. The resistive force during step-up and step-down and the assistive force during step-down are identified by black arrows in the leftmost panel. The green arrows in the third panel indicate changes in the contribution of chemical interactions. (c) Topography recorded along its sliding path where zero is defined as the position of the tip on the lower terrace. All friction tests were conducted with a single AFM probe with an applied normal force of 23.5 nN.

probe cantilever was calibrated following Sader's method.[32] The lateral sensitivity of the cantilever and detector was calculated by comparing the measured lateral signal (with mV units) on a reference sample with the known coefficient of friction (COF).[30] The reference sample was a Si wafer coated with diamond-like carbon, and the COF was about 0.15 in *n*-pentanol vapor.[33] Each of the lateral force and vertical position profiles was the average of 128 scans at the same location. The friction tests were carried out at room temperature (22−25 °C). A mixture vapor of dry N_2 and alcohol vapor flowed through the sample chamber. P/P_{sat} of the alcohol vapor was controlled via the ratio between the dry N_2 and the saturated alcohol vapor.[34] The alcohol used here includes methanol (Sigma-Aldrich, 99.8%) and *n*-pentanol (Sigma-Aldrich, ≥99%). The dry N_2 used in our experiments had a dew point of about −35 °C, meaning that the water concentration was 200−300 ppm.

Characterization of the Adsorbed Molecules on Graphite Surfaces. The adsorption of methanol and *n*-pentanol on the freshly exfoliated graphite surface was analyzed with polarization modulation reflection−absorption infrared spectroscopy (PM-RAIRS). PM-RAIRS analysis was carried out using a Thermo Nicolet Nexus 670 spectrometer equipped with a custom-designed reflection−absorption unit consisting of a ZnSe PM crystal, an environment control chamber, and an MCT-A detector.[35] The PM operation was performed using a photoelectric modulator (HINDS Instruments PEM-90) and a demodulator (GWC Instruments). The IR beam incidence angle was 81° from the surface normal. The PM-RAIRS spectra of the graphite surface were normalized with the spectrum of a clean gold surface obtained in dry N_2 to remove the Bessel function shape background from the phase demodulation process. The environment control was the same as that in the nanoscale friction measurement.

Reactive MD Simulations. Reactive MD simulations were used to model a silica tip sliding across a single-layer graphene step edge from the upper terrace to the lower terrace and back. The graphene step edge had an armchair structure, and four model systems with different edge terminations were created (see Figure S1 in the Supporting Information). The first model system mimicked the measurement performed in dry nitrogen conditions by terminating the step edge with alternating hydrogen and OH groups and the silica tip with OH groups. The second model system mimicked the experimental measurement performed in methanol vapor with a graphene step edge terminated with alternating hydrogen and methoxy groups and the silica tip terminated with methoxy groups. The third model system imitated the experimental measurement performed in *n*-pentanol vapor by modeling a graphene step edge terminated with alternating hydrogen and pentoxy groups. To ensure that the model tip size was comparable to the other cases, the silica tip was terminated with methoxy groups. Finally, the fourth system simulated sliding on a buried step edge, where a graphene layer covered a nonpassivated step edge.

The simulations used the ReaxFF[36] force field with a set of parameters previously developed[37] from a combination of parameters for C/H/O[38,39] and Si/C[40] interactions. The amorphous silica structure of the tip was created by heating cristobalite to 4000 K and then quenching to room temperature at a rate of 0.02 K/fs.[30,41] To increase computational efficiency, the tip was created in a semicircular disc shape, with a curvature (radius), thickness, and height of 2.5, 1.5, and 1.5 nm, respectively. As for the graphite surface, only three layers of graphene were considered and only the top two layers were deformable both at the upper and lower graphite basal planes. The substrate dimensions were 9.8 nm in the sliding direction (*x*-direction), 4.2 nm perpendicular to the sliding direction on the basal plane (*y*-direction), and about 1.0 nm normal to the graphite basal plane (*z*-direction).

Each simulation was performed in four different steps: (i) initial energy minimization and equilibrium until the potential energy reached a steady state, (ii) vertical displacement of the tip toward the substrate at a speed of 10 m/s until the minimum distance between the tip and substrate reached 0.3 nm, (iii) application of 10 nN normal force to the top rigid part of the tip for 120 ps, which corresponds to about 5.0 GPa pressure based on the DMT model,[31] and (iv) dragging the tip in the sliding direction (perpendicular to the step edge) at a speed of 10 m/s using a harmonic spring with a 6 N/m stiffness constant. The canonical ensemble was employed with a

https://dx.doi.org/10.1021/acsami.0c08121
ACS Appl. Mater. Interfaces 2020, 12, 30007−30015

Langevin thermostat to maintain the temperature at 300 K throughout the simulations. The velocity of the atoms in the sliding direction was excluded from the temperature calculation used by the thermostat. During the sliding process, the lateral force was calculated as the sum of the forces on all of the tip atoms in the sliding direction. To reduce the noise in the lateral force, averages were taken every 0.1 ps. All of the simulations were performed using the large atomic/molecular massively parallel simulation (LAMMPS) code,[42] and OVITO software[43] was used to visualize the results.

RESULTS AND DISCUSSION

AFM-Based Single-Asperity Friction Measurement. Figure 2a illustrates the AFM-based single-asperity friction tests. The Si tip used for AFM measurements had a native oxide layer terminated with silanol groups due to UV/ozone cleaning.[34] The exposed graphene step edges were terminated with H atoms and OH groups due to reactions with water molecules in the gas phase during mechanical exfoliation in ambient air.[20,21] In case (i), the nanoscale friction tests were performed in dry nitrogen, where transient H-bonding interactions can occur between the tip and the step edge (Figure 2a,i).[30] In case (ii), friction tests were performed in alcohol vapor conditions.[44,45] We tested two alcohols with different alkyl chain lengths—methanol (Figure 2a,ii-α) and *n*-pentanol (Figure 2a,ii-β). In these two cases, H-bond formation between the tip and the step edge is suppressed because the alcohol molecules readily adsorb on the native silicon oxide surface,[46] covering the silanol groups. As shown in Figure 3, the C−H stretching vibration signals in the PM-

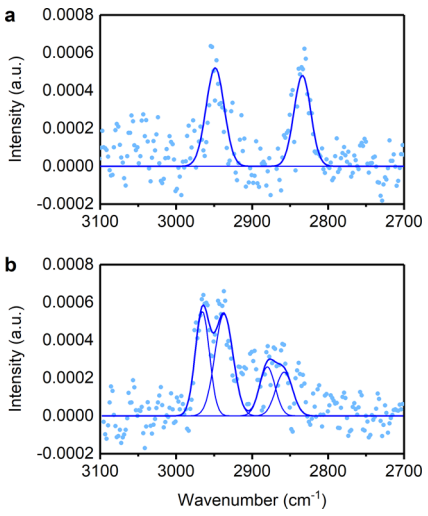

Figure 3. PM-RAIRS spectra on the graphite surface. Spectra were taken in (a) methanol vapor and (b) *n*-pentanol vapor at P/P_{sat} = 80%. The raw spectra obtained from 4000 scans are shown as symbols, and the fit results are shown as lines.

RAIRS spectra collected in alcohol vapor verify that alcohol molecules adsorb on the HOPG surface that consists primarily of graphite basal planes and a small number of steps. The OH-terminated step edges should be the primary sites for alcohol adsorption because of the H-bonding interactions. By comparing the spectra of graphite and Au in the same environmental conditions, we confirmed that, at 80% relative partial pressure of alcohol with respect to its saturation (P/P_{sat}), the number of alcohol molecules adsorbed on the graphite surface was less than a monolayer but far exceeds what is needed to fully cover the step edge sites (see Figure S2). If physisorbed molecules are removed due to the shear or sliding action, molecules impinging from the gas phase instantaneously replenish the vacant sites.[45] Thus, the adsorption of alcohol molecules on the sliding surfaces can be assumed to remain constant. In case (iii), friction was measured on a buried step edge (Figure 2a,iii) with the same height (0.34 nm) that was nearly parallel to the nearby exposed step edge (see Figure S3). Thus, friction forces were measured for both exposed and buried step edges with the same AFM tip under identical applied load and sliding speed conditions in different environments (dry nitrogen, methanol vapor, and *n*-pentanol vapor).

Figure 2b shows the lateral force measured with an applied normal force of 23.5 nN. Each of the lateral force profiles is the average of data collected from 128 scans at the same location (see Figure S4). Adhesion measured before and after the friction tests remained unchanged (see Figure S5), indicating minimal wear of the tip. Data collected at other normal forces (7.8 and 15.7 nN) are shown in Figure S6 and exhibit similar trends. During the step-up scan, a positive lateral force means resistance to the sliding motion of the AFM tip, and a negative lateral force corresponds to assistance to the motion. During the step-down scan, because the sliding direction is reversed, the sign of the lateral force has the opposite meaning; i.e., negative is resistive and positive is assistive. The three components of the lateral force signal, i.e., step-up resistive, step-down resistive, and step-down assistive, are identified with black arrows in Figure 2b,i.

In dry nitrogen (case i), there is a strong resistive force as the AFM tip ascends the OH-terminated step, while the friction behavior during the step-down process is the superposition of a broad resistive force and a sharp assistive force.[25,29] According to a previous study,[30] the step-up resistive component is due to the combined effects of the topographic height increase and the transient H-bond formation at the step, the step-down resistive component originates from the H-bonding interactions, and the step-down assistive component is caused by the height decrease. Interestingly, the magnitude of the step-up resistive component is much larger than the sum of the magnitudes of the step-down assistive and step-down resistive components. As shown in Figure S4, the lateral force during each scan begins to increase at the same location, which indicates that the step edge is not damaged by the repeated scans, so the OH coverage does not change over time and the resistive force induced by H-bonding is expected to be the same (at least similar) for both step-up and step-down scans. Therefore, it can be deduced that, in the presence of H-bonding interactions, the topography-induced resistive force during step-up is much larger than the topography-induced assistive force during step-down. In contrast, for the case of the buried step edge (case iii), where there is no chemical interaction so the step-down resistive component is zero, the magnitudes of the step-up resistive and step-down assistive forces are the same within the experimental error. Based on these observations, one may hypothesize that the topography effect during the step-up process is magnified by the H-bonding interaction at the graphene step edge.[30]

However, this hypothesis is not fully supported by the results of friction tests conducted in methanol or *n*-pentanol vapor (case ii). When the environmental condition is switched from dry nitrogen to methanol vapor (case ii-α), the magnitudes of both step-up resistive and step-down resistive components decrease. When the environment is switched to *n*-

https://dx.doi.org/10.1021/acsami.0c08121
ACS Appl. Mater. Interfaces 2020, 12, 30007−30015

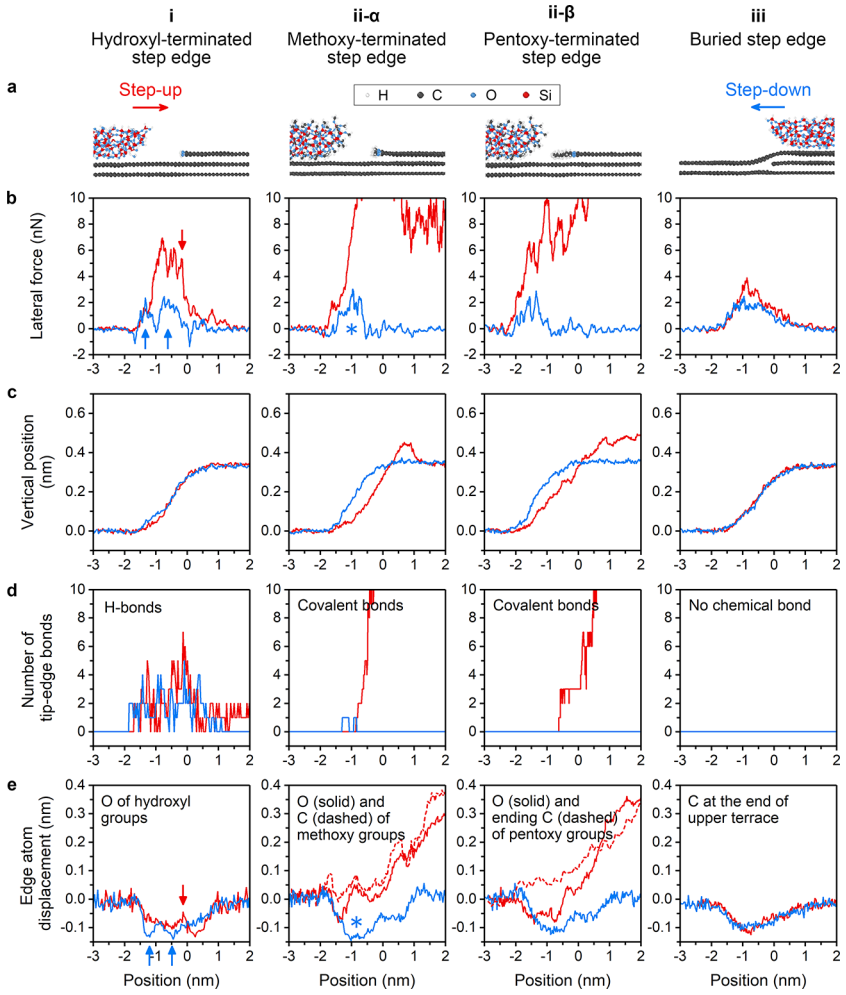

Figure 4. Reactive MD simulations of a silica tip sliding over a single-layer graphene step edge. (a) Close-up, side-view snapshots of the different models: (i) silanol-terminated tip on OH-terminated exposed step edge, (ii-α) methoxy-terminated tip on methoxy-terminated exposed step edge, (ii-β) methoxy-terminated tip on pentoxy-terminated exposed step edge, and (iii) silanol-terminated tip on buried step edge. (b) Lateral force and (c) vertical position of the tip. (d) Number of hydrogen or covalent bonds between the tip and the graphene step edge. (e) Average displacement of the carbon and/or oxygen atoms at the graphene step edge (see Figure S1 for the exact location of the atoms) where the abscissa refers to the lateral position of the center of the tip with respect to the step edge. The data collected during step-up are in red and during step-down are in blue. The arrows and asterisks are shown to guide the discussion in the main text.

pentanol vapor (case ii-β), there is a larger decrease in the step-up resistive and step-down resistive components (green arrows in Figure 2b,ii-β); in fact, the step-down resistive component becomes negligible. This indicates that the adsorbed alcohol molecules can suppress the transient H-bonding interaction between the Si tip and the exposed graphene step edge. The observation that the resistive force in methanol vapor is larger than that in *n*-pentanol could mean that the methyl group is not large enough to fully suppress the H-bonding interactions. Regardless, for both cases with and without H-bonding interactions, the magnitude of the step-up resistive force is much larger than that of the step-down assistive force.

The height profile recorded during the contact scan is plotted in Figure 2c. For the exposed graphene step edges (cases i, ii-α, and ii-β), the step-up profile has a smaller slope compared to the step-down profile, resulting in a hysteresis between step-up and step-down. This hysteresis is not observed for the buried step edge (case iii). Thus, the hysteresis in the recorded topography cannot be attributed to an artifact caused by the feedback control during the AFM scan across the topographic feature with the 0.34 nm height. Rather, it must be related to the large difference in the magnitude of the step-up resistive force and the step-down assistive force. In AFM, the recorded topography is the vertical trajectory of the upper part of the tip attached to the cantilever, not the position of the lower end of the tip in contact with the sample. The exact position of the tip apex in contact with the surface is difficult to determine; thus, the AFM height profiles cannot provide a definitive explanation for the friction hysteresis at the exposed step edges.

Reactive MD Simulations. MD simulations were performed to explain why the magnitude of the step-up resistive force is larger than that of the step-down assistive force for the exposed step edges with various chemical functionalities—hydrophilic OH groups and hydrophobic alkoxide groups. As shown in Figures 4a and S1, four model systems mimicked the four experimental cases. To model the friction tests in dry nitrogen, the silica tip was terminated with silanol groups (cases i and iii) and the exposed graphene step edge was terminated with H atoms and OH groups alternately (case i). To model the friction tests in methanol or *n*-pentanol vapor, where alcohol molecules adsorb on both the AFM tip

https://dx.doi.org/10.1021/acsami.0c08121
ACS Appl. Mater. Interfaces 2020, 12, 30007−30015

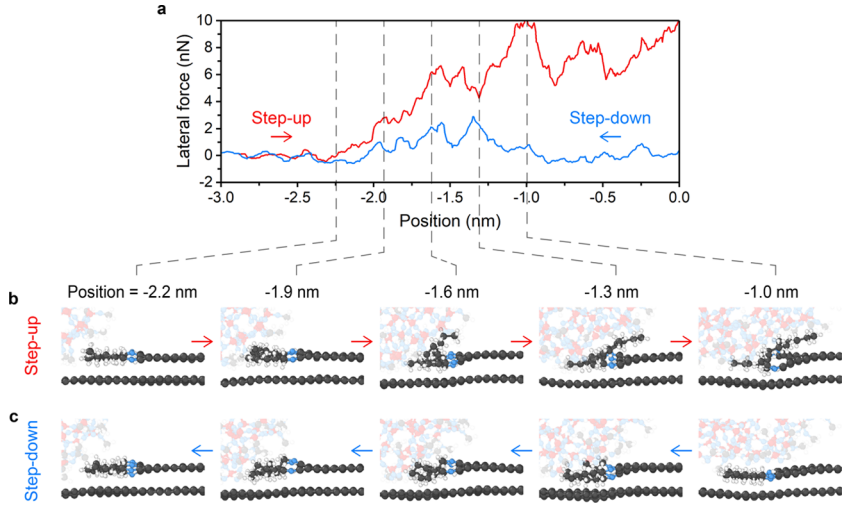

Figure 5. Anisotropic deformation of the pentoxy groups at the graphene step edge. (a) Lateral force from simulations of the pentoxy-terminated step edge (case ii-β). Side-view snapshots of the MD simulation showing the deformation of the pentoxy groups at the step edge during the (b) step-up and (c) step-down processes. Tip atoms are faded to highlight the behavior of the step edge.

and the graphene step edge, the silanol groups on the silica tip surface were approximated by methoxy groups and the OH groups at the exposed graphene step edge were replaced with methoxy groups or pentoxy groups (cases ii-α and ii-β). This strategy of modeling alkoxide groups to terminate the tip surface and the step edge was adopted to capture the important chemical features of the four cases with model systems small enough to simulate using reactive MD.

As shown in Figure 4b, the lateral force obtained from MD simulations exhibits similar trends as measured in the AFM experiments. First, the resistive force during step-up is much larger than the assistive force during step-down for the OH-terminated step edge (Figure 4b,i), whereas these assistive and resistive forces have similar magnitudes for the buried step edge (Figure 4b,iii). Further, there are clearly identifiable resistive peaks during step-down for the OH-terminated graphene step (case i) that are not present for the buried step edge (case iii). Finally, the step-down resistive force is smaller for the methoxy-terminated and pentoxy-terminated graphene step edges (Figure 4b,ii-α and ii-β) than for the OH-terminated edge. These trends are consistent with the experimental results shown in Figure 2b. However, unlike the experiments, the simulation results predict the step-up resistive force can be significantly larger for the methoxy-terminated and pentoxy-terminated graphene step edges than the OH-terminated step edge. The simulated lateral force eventually drops back to the basal plane value when the tip moves far enough from the step (see Figure S7). Despite this difference, the simulations capture the key trends of the experiments and therefore will be analyzed to understand the mechanisms underlying those trends.

Figure 4c shows the vertical position of the center of mass of the amorphous silica tip in the MD simulations. For the buried step edge (case iii), the tip trajectories during the step-up and step-down processes are identical. For the OH-terminated step edge (case i), there is a small hysteresis between the step-up and step-down trajectories. For the methoxy-terminated (cases ii-α) and pentoxy-terminated (case ii-β) graphene step edges, there is hysteresis between the step-up and step-down trajectories and the slope of the step-up trajectory is slightly smaller than that for step-down, consistent with the experimental measurements. This hysteresis indicates that the location at which the tip starts ascending the step edge differs from the location at which the tip finishes descending the step edge. The main difference from the experiments is that the simulated tip trajectory reaches a final position much higher than the upper terrace, although it eventually comes back to the level of the upper terrace (as shown in case ii-α). This is attributable to the difference between the chemisorbed alkoxide groups in simulations and the physisorbed alcohol in AFM experiments (discussed later along with Figure 5).

Figure 4d shows the transient chemical bonds formed between the tip and the step edge. As expected, there are several transient H-bonds formed between the OH-terminated silica tip and the OH-terminated step edge during both step-up and step-down processes (case i), while there are no chemical bonds between the tip and the buried step edge (case iii). For the methoxy-terminated (case ii-α) and pentoxy-terminated (case ii-β) graphene step edges, there are no chemical interactions between the tip and the step edge during the step-down process. However, covalent bonding is observed during the step-up process for these two cases. As the tip ascends the step, initially, the friction increases, but there is no bonding. However, when the tip is partially up the step, there is a sharp increase of covalent bonding for both the methoxy-terminated and pentoxy-terminated graphene step edges. The origin and implications of this covalent bonding in methoxy (ii-α) and pentoxy (ii-β) cases will be discussed later.

The degree of physical deformation or deflection of functional groups during the scan was quantified from the displacement of individual atoms at the step edge in the simulations. Figure 4e shows the average displacement of the carbon and/or oxygen atoms at the graphene step edges (atoms being tracked are identified in Figure S1). For the buried step edge (case iii), the terminal carbon atoms are deflected downward by almost the same magnitude during step-up and step-down. For the OH-terminated step edge (case i), the maximum downward deflection is similar for step-up and step-down, but they occur at different lateral positions. This trend can be attributed to the transient H-bonds (Figure 4d,i) and their effect on the tip trajectory (Figure 4c,i). Specifically, as the tip ascends the step, it is pulled down due to

https://dx.doi.org/10.1021/acsami.0c08121
ACS Appl. Mater. Interfaces 2020, 12, 30007−30015

H-bonding with the surface OH groups; at the same time, the step-edge OH groups H-bonded to the tip are pulled up slightly.[30] Such upward bending of $H-O-C_{graphene}$ could cause a large resistive force (see, for example, the red arrows in Figure 3 4b,i and e,i). Quantitative correlations between H-bonding, deflection, and friction could not be drawn because the calculated friction force is the sum of various processes stochastically occurring over a specific time frame and location in MD simulations. Nonetheless, the qualitative correlation suggests that local deformation of the terminal groups at the topographic step, which is coupled with transient chemical interactions with the countersurface, plays a critical role in determining the magnitude of friction.

In the first part of the simulated step-up processes for the methoxy-terminated (case ii-α) and pentoxy-terminated (case ii-β) step edges, no covalent bonds are formed between the tip and the step edge (i.e., before −0.8 nm in Figure 4ii-α and ii-β). In this region, the terminal carbon atoms of the alkoxide groups are pushed upward, while their oxygen atoms are pushed downward. This means that the alkoxide groups are highly deformed or physically strained from their equilibrium conformations. To show this clearly, the deformation of pentoxy groups (case ii-β) is analyzed in Figure 5; the lateral force is replotted for this case in Figure 5a. A series of snapshots from the MD simulations during the step-up process are shown in Figure 5b. Initially, only the terminal methyl group is bent upward, but gradually the whole pentoxy group is bent up as the tip travels further toward the upper terrace. Similar behavior was observed for the methoxy group in case ii-α. Thus, it can be concluded that the physical deformation of the alkoxide group is the main cause of the high friction during the step-up process in this region. A similar process is likely to occur for the physisorbed alcohol molecules in the AFM experiment. Such severe deformation does not occur during the step-down process; only small and gradual downward deformations are observed (see Figure 5c). These results indicate that the difference in lateral force associated with the anisotropic deflection of the alkyl groups at the graphene step edge is the origin of the friction hysteresis between step-up and step-down.

Deflection of the alkyl groups at the step edge also explains the chemical bonding that dominates the lateral force behavior in the latter part of the step-up process (tip lateral position > 0.8 nm) for the methoxy-terminated and pentoxy-terminated step edges (Figure 4d,ii-α and ii-β). In this region, the chemisorbed alkoxide groups are substantially deformed so that chemical reactions occur between the deformed alkoxide groups and the countersurface. It is known that the shear-induced physical deformation of chemisorbed molecules can lower reaction barriers, thereby facilitating chemical reactions that normally do not happen in thermal reaction conditions.[41,47] This is called a tribochemical reaction.[48−51] Based on the high degree of strain in the molecular conformation of pentoxy group that can be seen in the last frame of Figure 5b, one can imagine that further deformation will destabilize the pentoxy group enough to cause the dissociation of the $O_{pentoxy}-C_{graphene}$ bonds at the step edge and the formation of new chemical bonds with the countersurface. Subsequently, the position of the oxygen atom of the alkoxide group follows the trajectory of the terminal carbon atom. Such tribochemical processes may not occur readily for the physisorbed molecules because they can be pushed to a lower pressure zone in the contact area.[47] Since the decrease in the resistive force magnitude during step-up is similar to the decrease in resistive force during step-down in our experiments (see green arrows in Figure 2b,ii-β), it is unlikely that the physisorbed alcohol molecules are completely squeezed out of the contact region, which would allow direct H-bonding between the tip and the step edge.

During the step-down process in all four cases, the edge atoms are pushed downwards (Figure 4e). Taking a closer look at the buried step edge (case iii), the step-down assistive force correlates well with, almost mirroring, the downward deflection of the edge atom. In the OH-terminated (case i) and methoxy-terminated (case ii-α) step edges, the locations of large assistive force in Figure 4b also closely coincide with tip positions where the downward deflection of the edge atoms is large in Figure 4e (marked with blue arrows in case i and asterisks in case ii-α). In the pentoxy-terminated step edge (case ii-β), the positions of small spikes in the assistive force during step-down correspond with positions where the pentyl groups are highly kinked (for instance, see three snapshots at −2.0, −1.6, and −1.3 nm in Figure 5c). All of these observations suggest that the elastic recovery of the deformed moieties at the step edge exerts an assistive force that pushes the tip along the descending direction.

The observations made here based on AFM measurements and MD simulations of an ideal graphene step edge have practical implications for real engineering materials and systems. For example, these results explain the environmental sensitivity of hydrogenated diamond-like carbon (H-DLC).[52−56] In dry nitrogen, H-DLC exhibits superlubricity with a friction coefficient lower than 0.01 after the initial run-in period.[52] During run-in, the oxidized surface layer wears off[56] and the material in the sliding interface becomes graphitic.[57] Such graphitic layers are neither highly crystalline nor atomically flat,[58,59] likely exhibiting step-edge-like defects. If such defects are chemically inert or deform reversibly, they would not increase friction significantly (similar to case iii). When H-DLC friction is measured in humid air, the formation of OH groups is inevitable due to reactions of dangling bonds with water molecules impinging from the gas phase. The H-bonding interactions at the edges of graphitic layers will cause high friction (similar to case i), which could be a reason that H-DLC loses its superlubricity in ambient air. Even if H-DLC friction is measured in alcohol vapor environments, which can suppress the H-bonding interactions,[55] the superlubricity is lost due to the anisotropic deformation of alcohol molecules or alkoxide groups at the edges of sliding graphitic layers (similar to case ii). The present study has shown that both chemical interactions and physical deflection must be mitigated to obtain ultralow friction, suggesting new directions in surface engineering.

CONCLUSIONS

By comparing single-asperity friction at chemically inert and active graphene step edges on the graphite basal plane, the physical and chemical contributions to friction at the nanoscale have been successfully identified. It is found that the friction at an exposed step edge is reduced in an alcohol vapor because the adsorbed alcohol molecules can suppress the H-bonding between the step edge and the countersurface. However, even if the chemical contribution to friction is eliminated, because of the anisotropic deformation of the terminal groups at the exposed step edge, the friction of an exposed step edge is still higher than that of a buried step edge. More generally, it is

https://dx.doi.org/10.1021/acsami.0c08121
ACS Appl. Mater. Interfaces 2020, 12, 30007−30015

demonstrated that, within one cycle of a tip sliding up and down a topographic step, the energy consumed during the step-up process can be restored during the step-down process only if (a) there is no chemical interaction between the tip and the step and (b) the deflection of the step is identical during the step-up and step-down processes. Otherwise, there will be a net energy loss when shear occurs at a topographically corrugated interface, leading to an increase in friction. This nanoscale mechanism can be used to explain friction at larger scales where the sliding surfaces are neither atomically smooth nor chemically inert.

■ ASSOCIATED CONTENT

Supporting Information

The Supporting Information is available free of charge at https://pubs.acs.org/doi/10.1021/acsami.0c08121.

MD simulation models; PM-RAIRS spectra of alcohol vapors and adsorption on Au surface; topography and lateral signal on graphite surfaces; AFM lateral force at graphene step edges; AFM pull-off force on graphite basal plane before and after friction tests; full-range simulated lateral force at methoxy-terminated graphene step edge (PDF)

■ AUTHOR INFORMATION

Corresponding Authors

Ashlie Martini − *Department of Mechanical Engineering, University of California Merced, Merced, California 95343, United States;* orcid.org/0000-0003-2017-6081; Email: amartini@ucmerced.edu

Seong H. Kim − *Department of Chemical Engineering and Materials Research Institute, Pennsylvania State University, University Park, Pennsylvania 16802, United States;* orcid.org/0000-0002-8575-7269; Email: shkim@engr.psu.edu

Authors

Zhe Chen − *Department of Chemical Engineering and Materials Research Institute, Pennsylvania State University, University Park, Pennsylvania 16802, United States;* orcid.org/0000-0002-5874-7196

Arash Khajeh − *Department of Mechanical Engineering, University of California Merced, Merced, California 95343, United States;* orcid.org/0000-0002-9061-9370

Complete contact information is available at: https://pubs.acs.org/10.1021/acsami.0c08121

Author Contributions

§Z.C. and A.K. contributed equally to this work.

Author Contributions

S.H.K. and A.M. conceived the study. Z.C. performed the nanoscale friction measurement and analyzed the molecule adsorption. A.K. carried out the MD simulations. All authors contributed to the discussion of results and participated in the manuscript preparation.

Notes

The authors declare no competing financial interest.

■ ACKNOWLEDGMENTS

This work was supported by the National Science Foundation (Grant nos. CMMI-1727571 and 1727356).

■ REFERENCES

(1) Holmberg, K.; Erdemir, A. Influence of Tribology on Global Energy Consumption, Costs and Emissions. *Friction* **2017**, *5*, 263−284.

(2) Wang, Z. L. Triboelectric Nanogenerators as New Energy Technology for Self-Powered Systems and as Active Mechanical and Chemical Sensors. *ACS Nano* **2013**, *7*, 9533−9557.

(3) Chen, Z.; Liu, Y.; Gunsel, S.; Luo, J. Mechanism of Antiwear Property under High Pressure of Synthetic Oil-Soluble Ultrathin MoS_2 Sheets as Lubricant Additives. *Langmuir* **2018**, *34*, 1635−1644.

(4) Chen, H.; Zhang, L.; Zhang, D.; Zhang, P.; Han, Z. Bioinspired Surface for Surgical Graspers Based on the Strong Wet Friction of Tree Frog Toe Pads. *ACS Appl. Mater. Interfaces* **2015**, *7*, 13987−13995.

(5) Amontons, G. De la Resistance Cause'e dans les Machines. *Mem. Acad. R. A* **1699**, 275−282.

(6) Gao, J.; Luedtke, W. D.; Gourdon, D.; Ruths, M.; Israelachvili, J. N.; Landman, U. Frictional Forces and Amontons' Law: From the Molecular to the Macroscopic Scale. *J. Phys. Chem. B* **2004**, *108*, 3410−3425.

(7) Greenwood, J. A.; Williamson, J. P. Contact of Nominally Flat Surfaces. *Proc. R. Soc. London, Ser. A* **1966**, *295*, 300−319.

(8) Jacobs, T. D. B.; Martini, A. Measuring and Understanding Contact Area at the Nanoscale: A Review. *Appl. Mech. Rev.* **2017**, *69*, No. 060802.

(9) Mo, Y.; Turner, K. T.; Szlufarska, I. Friction Laws at the Nanoscale. *Nature* **2009**, *457*, 1116−1119.

(10) Luan, B.; Robbins, M. O. The Breakdown of Continuum Models for Mechanical Contacts. *Nature* **2005**, *435*, 929.

(11) Elinski, M. B.; Liu, Z.; Spear, J. C.; Batteas, J. D. 2D or Not 2D? The Impact of Nanoscale Roughness and Substrate Interactions on the Tribological Properties of Graphene and MoS_2. *J. Phys. D: Appl. Phys.* **2017**, *50*, No. 103003.

(12) Chen, Z.; Vazirisereshk, M. R.; Khajeh, A.; Martini, A.; Kim, S. H. Effect of Atomic Corrugation on Adhesion and Friction: A Model Study with Graphene Step Edges. *J. Phys. Chem. Lett.* **2019**, *10*, 6455−6461.

(13) Milne, Z. B.; Schall, J. D.; Jacobs, T. D. B.; Harrison, J. A.; Carpick, R. W. Covalent Bonding and Atomic-Level Plasticity Increase Adhesion in Silicon−Diamond Nanocontacts. *ACS Appl. Mater. Interfaces* **2019**, *11*, 40734−40748.

(14) Dienwiebel, M.; Verhoeven, G. S.; Pradeep, N.; Frenken, J. W. M.; Heimberg, J. A.; Zandbergen, H. W. Superlubricity of Graphite. *Phys. Rev. Lett.* **2004**, *92*, No. 126101.

(15) Feng, X.; Kwon, S.; Park, J. Y.; Salmeron, M. Superlubric Sliding of Graphene Nanoflakes on Graphene. *ACS Nano* **2013**, *7*, 1718−1724.

(16) Song, Y.; Mandelli, D.; Hod, O.; Urbakh, M.; Ma, M.; Zheng, Q. Robust Microscale Superlubricity in Graphite/Hexagonal Boron Nitride Layered Heterojunctions. *Nat. Mater.* **2018**, *17*, 894−899.

(17) Berman, D.; Erdemir, A.; Sumant, A. V. Graphene: A New Emerging Lubricant. *Mater. Today* **2014**, *17*, 31−42.

(18) Baykara, M. Z.; Vazirisereshk, M. R.; Martini, A. Emerging Superlubricity: A Review of the State of the Art and Perspectives on Future Research. *Appl. Phys. Rev.* **2018**, *5*, No. 041102.

(19) Liu, Y.; Song, A.; Xu, Z.; Zong, R.; Zhang, J.; Yang, W.; Wang, R.; Hu, Y.; Luo, J.; Ma, T. Interlayer Friction and Superlubricity in Single-Crystalline Contact Enabled by Two-Dimensional Flake-Wrapped Atomic Force Microscope Tips. *ACS Nano* **2018**, *12*, 7638−7646.

(20) Rietsch, J.-C.; Brender, P.; Dentzer, J.; Gadiou, R.; Vidal, L.; Vix-Guterl, C. Evidence of Water Chemisorption During Graphite Friction under Moist Conditions. *Carbon* **2013**, *55*, 90−97.

(21) Levita, G.; Restuccia, P.; Righi, M. C. Graphene and MoS_2 Interacting with Water: A Comparison by Ab Initio Calculations. *Carbon* **2016**, *107*, 878−884.

(22) Dong, Y.; Liu, X. Z.; Egberts, P.; Ye, Z.; Carpick, R. W.; Martini, A. Correlation between Probe Shape and Atomic Friction Peaks at Graphite Step Edges. *Tribol. Lett.* **2013**, *50*, 49−57.

(23) Egberts, P.; Ye, Z.; Liu, X. Z.; Dong, Y.; Martini, A.; Carpick, R. W. Environmental Dependence of Atomic-Scale Friction at Graphite Surface Steps. *Phys. Rev. B* **2013**, *88*, No. 035409.
(24) Ye, Z.; Otero-de-la-Roza, A.; Johnson, E. R.; Martini, A. Effect of Tip Shape on Atomic-Friction at Graphite Step Edges. *Appl. Phys. Lett.* **2013**, *103*, No. 081601.
(25) Chen, Z.; Kim, S. H. Measuring Nanoscale Friction at Graphene Step Edges. *Friction* **2020**, 1−10.
(26) Lang, H.; Peng, Y.; Zeng, X.; Cao, X.; Liu, L.; Zou, K. Effect of Relative Humidity on the Frictional Properties of Graphene at Atomic-Scale Steps. *Carbon* **2018**, *137*, 519−526.
(27) Ye, Z.; Martini, A. Atomic Friction at Exposed and Buried Graphite Step Edges: Experiments and Simulations. *Appl. Phys. Lett.* **2015**, *106*, No. 231603.
(28) Lee, H.; Lee, H.-B.-R.; Kwon, S.; Salmeron, M.; Park, J. Y. Internal and External Atomic Steps in Graphite Exhibit Dramatically Different Physical and Chemical Properties. *ACS Nano* **2015**, *9*, 3814−3819.
(29) Chen, L.; Chen, Z.; Tang, X.; Yan, W.; Zhou, Z.; Qian, L.; Kim, S. H. Friction at Single-Layer Graphene Step Edges Due to Chemical and Topographic Interactions. *Carbon* **2019**, *154*, 67−73.
(30) Chen, Z.; Khajeh, A.; Martini, A.; Kim, S. H. Chemical and Physical Origins of Friction on Surfaces with Atomic Steps. *Sci. Adv.* **2019**, *5*, No. eaaw0513.
(31) Derjaguin, B. V.; Muller, V. M.; Toporov, Y. P. Effect of Contact Deformations on the Adhesion of Particles. *J. Colloid Interface Sci.* **1975**, *53*, 314−326.
(32) Sader, J. E.; Larson, I.; Mulvaney, P.; White, L. R. Method for the Calibration of Atomic Force Microscope Cantilevers. *Rev. Sci. Instrum.* **1995**, *66*, 3789−3798.
(33) Barnette, A. L.; Ohlhausen, J. A.; Dugger, M. T.; Kim, S. H. Humidity Effects on in Situ Vapor Phase Lubrication with N-Pentanol. *Tribol. Lett.* **2014**, *55*, 177−186.
(34) Asay, D. B.; Kim, S. H. Evolution of the Adsorbed Water Layer Structure on Silicon Oxide at Room Temperature. *J. Phys. Chem. B* **2005**, *109*, 16760−16763.
(35) Díez-Pérez, I.; Luna, M.; Teherán, F.; Ogletree, D. F.; Sanz, F.; Salmeron, M. Interaction of Water with Self-Assembled Monolayers of Alkylsilanes on Mica. *Langmuir* **2004**, *20*, 1284−1290.
(36) Senftle, T. P.; Hong, S.; Islam, M. M.; Kylasa, S. B.; Zheng, Y.; Shin, Y. K.; Junkermeier, C.; Engel-Herbert, R.; Janik, M. J.; Aktulga, H. M.; Verstraelen, T.; Grama, A.; van Duin, A. C. T. The ReaxFF Reactive Force-Field: Development, Applications and Future Directions. *npj Comput. Mater.* **2016**, *2*, 15011.
(37) Chipara, A. C.; Tsafack, T.; Owuor, P. S.; Yeon, J.; Junkermeier, C. E.; van Duin, A. C. T.; Bhowmick, S.; Asif, S. A. S.; Radhakrishnan, S.; Park, J. H.; Brunetto, G.; Kaipparettu, B. A.; Galvão, D. S.; Chipara, M.; Lou, J.; Tsang, H. H.; Dubey, M.; Vajtai, R.; Tiwary, C. S.; Ajayan, P. M. Underwater Adhesive Using Solid−Liquid Polymer Mixes. *Mater. Today Chem.* **2018**, *9*, 149−157.
(38) Goverapet Srinivasan, S.; van Duin, A. C. T. Molecular-Dynamics-Based Study of the Collisions of Hyperthermal Atomic Oxygen with Graphene Using the ReaxFF Reactive Force Field. *J. Phys. Chem. A* **2011**, *115*, 13269−13280.
(39) Chenoweth, K.; van Duin, A. C. T.; Goddard, W. A. ReaxFF Reactive Force Field for Molecular Dynamics Simulations of Hydrocarbon Oxidation. *J. Phys. Chem. A* **2008**, *112*, 1040−1053.
(40) Chenoweth, K.; Cheung, S.; van Duin, A. C. T.; Goddard, W. A.; Kober, E. M. Simulations on the Thermal Decomposition of a Poly(Dimethylsiloxane) Polymer Using the ReaxFF Reactive Force Field. *J. Am. Chem. Soc.* **2005**, *127*, 7192−7202.
(41) Khajeh, A.; He, X.; Yeon, J.; Kim, S. H.; Martini, A. Mechanochemical Association Reaction of Interfacial Molecules Driven by Shear. *Langmuir* **2018**, *34*, 5971−5977.
(42) Plimpton, S. Fast Parallel Algorithms for Short-Range Molecular Dynamics. *J. Comput. Phys.* **1995**, *117*, 1−19.
(43) Alexander, S. Visualization and Analysis of Atomistic Simulation Data with Ovito−the Open Visualization Tool. *Modell. Simul. Mater. Sci. Eng.* **2010**, *18*, No. 015012.
(44) Barthel, A. J.; Al-Azizi, A.; Surdyka, N. D.; Kim, S. H. Effects of Gas or Vapor Adsorption on Adhesion, Friction, and Wear of Solid Interfaces. *Langmuir* **2014**, *30*, 2977−2992.
(45) Alazizi, A.; Barthel, A. J.; Surdyka, N. D.; Luo, J.; Kim, S. H. Vapors in the Ambient—a Complication in Tribological Studies or an Engineering Solution of Tribological Problems? *Friction* **2015**, *3*, 85−114.
(46) Asay, D. B.; Dugger, M. T.; Ohlhausen, J. A.; Kim, S. H. Macro- to Nanoscale Wear Prevention Via Molecular Adsorption. *Langmuir* **2008**, *24*, 155−159.
(47) Khajeh, A.; Chen, Z.; Kim, S. H.; Martini, A. Effect of Ambient Chemistry on Friction at the Basal Plane of Graphite. *ACS Appl. Mater. Interfaces* **2019**, *11*, 40800−40807.
(48) Zhang, J.; Ewen, J. P.; Ueda, M.; Wong, J. S. S.; Spikes, H. A. Mechanochemistry of Zinc Dialkyldithiophosphate on Steel Surfaces under Elastohydrodynamic Lubrication Conditions. *ACS Appl. Mater. Interfaces* **2020**, *12*, 6662−6676.
(49) Gosvami, N. N.; Bares, J. A.; Mangolini, F.; Konicek, A. R.; Yablon, D. G.; Carpick, R. W. Mechanisms of Antiwear Tribofilm Growth Revealed in Situ by Single-Asperity Sliding Contacts. *Science* **2015**, *348*, 102.
(50) Garvey, M.; Weinert, M.; Tysoe, W. T. On the Pressure Dependence of Shear Strengths in Sliding, Boundary-Layer Friction. *Tribol. Lett.* **2011**, *44*, 67.
(51) Martini, A.; Eder, J. S.; Dörr, N. Tribochemistry: A Review of Reactive Molecular Dynamics Simulations. *Lubricants* **2020**, *8*, No. 44.
(52) Erdemir, A. Genesis of Superlow Friction and Wear in Diamondlike Carbon Films. *Tribol. Int.* **2004**, *37*, 1005−1012.
(53) Eryilmaz, O. L.; Erdemir, A. Surface Analytical Investigation of Nearly-Frictionless Carbon Films after Tests in Dry and Humid Nitrogen. *Surf. Coat. Technol.* **2007**, *201*, 7401−7407.
(54) Eryilmaz, O. L.; Erdemir, A. TOF-SIMS and XPS Characterization of Diamond-Like Carbon Films after Tests in Inert and Oxidizing Environments. *Wear* **2008**, *265*, 244−254.
(55) Marino, M. J.; Hsiao, E.; Chen, Y.; Eryilmaz, O. L.; Erdemir, A.; Kim, S. H. Understanding Run-in Behavior of Diamond-Like Carbon Friction and Preventing Diamond-Like Carbon Wear in Humid Air. *Langmuir* **2011**, *27*, 12702−12708.
(56) Al-Azizi, A. A.; Eryilmaz, O.; Erdemir, A.; Kim, S. H. Surface Structure of Hydrogenated Diamond-Like Carbon: Origin of Run-in Behavior Prior to Superlubricious Interfacial Shear. *Langmuir* **2015**, *31*, 1711−1721.
(57) Manimunda, P.; Al-Azizi, A.; Kim, S. H.; Chromik, R. R. Shear-Induced Structural Changes and Origin of Ultralow Friction of Hydrogenated Diamond-Like Carbon (DLC) in Dry Environment. *ACS Appl. Mater. Interfaces* **2017**, *9*, 16704−16714.
(58) Wang, D.-S.; Chang, S.-Y.; Huang, Y.-C.; Wu, J.-B.; Lai, H.-J.; Leu, M.-S. Nanoscopic Observations of Stress-Induced Formation of Graphitic Nanocrystallites at Amorphous Carbon Surfaces. *Carbon* **2014**, *74*, 302−311.
(59) Chen, X.; Zhang, C.; Kato, T.; Yang, X.-A.; Wu, S.; Wang, R.; Nosaka, M.; Luo, J. Evolution of Tribo-Induced Interfacial Nanostructures Governing Superlubricity in a-C:H and a-C:H:Si Films. *Nat. Commun.* **2017**, *8*, No. 1675.

https://dx.doi.org/10.1021/acsami.0c08121
ACS Appl. Mater. Interfaces 2020, 12, 30007−30015